Targeting of c-MET and AXL by cabozantinib is a potential therapeutic strategy for patients with head and neck cell carcinoma

Anais Hagege, Esma Saada-Bouzid, Damien Ambrosetti, Olivia Rastoin, Julien Boyer, Xingkang He, Julie Rousset, Christopher Montemagno, Jérome Doyen, Florence Pedeutour, et al.

Cell Reports
Medicine

Article

Targeting of c-MET and AXL by cabozantinib is a potential therapeutic strategy for patients with head and neck cell carcinoma

Graphical abstract

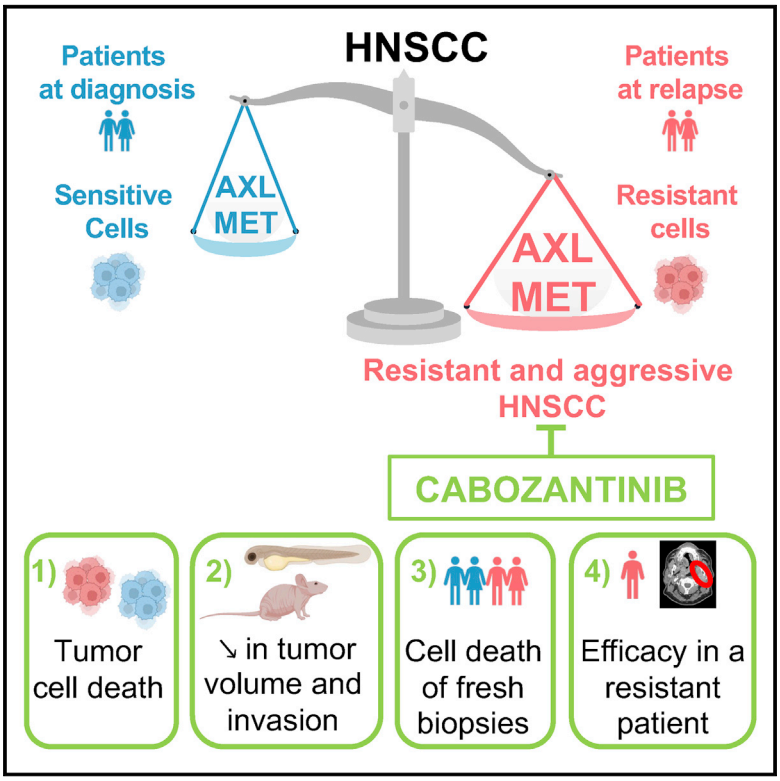

Highlights

- AXL and c-MET are overexpressed in radiotherapy- and cisplatin-resistant HNSCC
- Overexpression of AXL and c-MET contributes to tumor aggressiveness and poor prognosis
- Cabozantinib has anti-tumor and anti-metastatic efficacy in mice and zebrafish models
- Cabozantinib efficacy is shown on HNSCC biopsies and in one patient after several relapses

Authors

Anais Hagege, Esma Saada-Bouzid, Damien Ambrosetti, ..., Yihai Cao, Gilles Pagès, Maeva Dufies

Correspondence

maeva.dufies@gmail.com

In brief

Hagege et al. describe that AXL and c-MET are overexpressed in radio- and/or cisplatin HNSCC cells and patients and represent new potential therapeutic targets. Their inhibitor, cabozantinib, shows its efficacy in resistant *in vitro* and *in vivo* models, in 3D sections of HNSCC biopsies, and in one resistant patient.

Hagege et al., 2022, Cell Reports Medicine *3*, 100659
September 20, 2022
https://doi.org/10.1016/j.xcrm.2022.100659

CellPress

Cell Reports Medicine

CellPress
OPEN ACCESS

Article

Targeting of c-MET and AXL by cabozantinib is a potential therapeutic strategy for patients with head and neck cell carcinoma

Anais Hagege,[1,2] Esma Saada-Bouzid,[4] Damien Ambrosetti,[5] Olivia Rastoin,[1,2] Julien Boyer,[4] Xingkang He,[6] Julie Rousset,[3] Christopher Montemagno,[1,2,6] Jérome Doyen,[1,4] Florence Pedeutour,[1,3] Julien Parola,[1,2,4] Isabelle Bourget,[1] Frederic Luciano,[1,2] Alexandre Bozec,[4] Yihai Cao,[6] Gilles Pagès,[1,2,7,8] and Maeva Dufies[1,2,7,8,9,*]

[1]University Côte d'Azur, CNRS UMR 7284, INSERM U1081, Centre Antoine Lacassagne, Institute for Research on Cancer and Aging of Nice (IRCAN), 06189 Nice, France

[2]Laboratoire International Associé Université Côte d'Azur, Centre Scientifique de Monaco, LIA ROPSE, Monaco, Principality of Monaco

[3]Laboratory of Solid Tumor Genetics, University Hospital of Nice Côte d'Azur, Nice, France

[4]University Côte d'Azur, Centre Antoine Lacassagne, 06189 Nice, France

[5]Hôpital Pasteur, Central Laboratory of Pathology, University Côte d'Azur, Centre Hospitalier Universitaire (CHU) de Nice, 06000 Nice, France

[6]Department of Microbiology, Tumor and Cell Biology, Karolinska Institutet, 171 77 Stockholm, Sweden

[7]Biomedical Department, Centre Scientifique de Monaco, 98000 Monaco, Principality of Monaco

[8]These authors contributed equally

[9]Lead contact

*Correspondence: maeva.dufies@gmail.com

https://doi.org/10.1016/j.xcrm.2022.100659

SUMMARY

Local or metastatic relapse following surgery, radiotherapy, and cisplatin is the leading cause of death in patients with head and neck squamous cell carcinoma (HNSCC). Our study shows overexpression of c-MET and AXL in HNSCC cells and patients resistant to radiotherapy and cisplatin. We demonstrate that cabozantinib, an inhibitor of vascular endothelial growth factor receptor (VEGFR), c-MET, and AXL, decreases migration, invasion, and proliferation and induces mitotic catastrophe and apoptotic cell death of naive and radiotherapy- and cisplatin-resistant HNSCC cells. Cabozantinib inhibits the growth and metastatic spread of experimental HNSCC in zebrafish and the growth of experimental HNSCC in mice by blocking tumor cell proliferation and angiogenesis. The efficacy of cabozantinib is also confirmed on viable sections of surgically removed specimens of human HNSCC and on a patient who relapses after five lines of treatment. These results suggest that cabozantinib is relevant for the treatment of patients with HNSCC after relapse under radiotherapy and cisplatin.

INTRODUCTION

Head and neck squamous cell carcinomas (HNSCCs) are the sixth most common cancers worldwide, accounting for nearly 6% of all cancers, with two-thirds of cases occurring in developing countries.

Tobacco and alcohol dependence and human papillomavirus (HPV) infection are risk factors for developing HNSCC.

HNSCC kills more than 140,000 patients each year after relapse following surgery, radiotherapy, chemotherapy, or a combination of radio- and chemotherapy. Recurrence occurs in 30%–50% of patients due to acquired resistance to conventional treatments, leading to patient death within a few months. In addition, the radiotherapy-dependent destruction of the salivary glands severely limits the quality of life of cured patients. FDA-approved therapies include methotrexate, 5-fluorouracil, bleomycin, cisplatin, cetuximab, docetaxel, and, more recently, immunotherapy (anti-PD-1, pembrolizumab, or nivolumab).[1,2]

High levels of vascular endothelial growth factor (VEGF) and its receptors (VEGFR1/2/3) are frequently observed in HNSCCs and correlate with shorter survival.[3] Therefore, high levels of VEGF in HNSCC may play a radioprotective role, reducing the efficacy of radiotherapy and contributing to relapse.[4,5] Anti-angiogenic therapies may enhance the effect of radiotherapy on the tumor vasculature.[6]

In addition to the involvement of angiogenesis in HNSCC, lymphangiogenesis plays an important role in the aggressiveness of this pathology since lymph node invasion represents the main pathway for metastatic spread of HNSCC. Lymphangiogenesis is the most significant detrimental prognostic indicator for these cancers.[7]

VEGFC and VEGFD are the main "drivers" of lymphangiogenesis. High levels correlate with lymphatic vessel density, lymph node metastasis, and poor prognosis in HNSCC. We have previously shown that radiotherapy stimulates VEGFC expression in HNSCC cells, resulting in increased aggressiveness (ability to form fast-growing experimental tumors when injected into nude mice).[8]

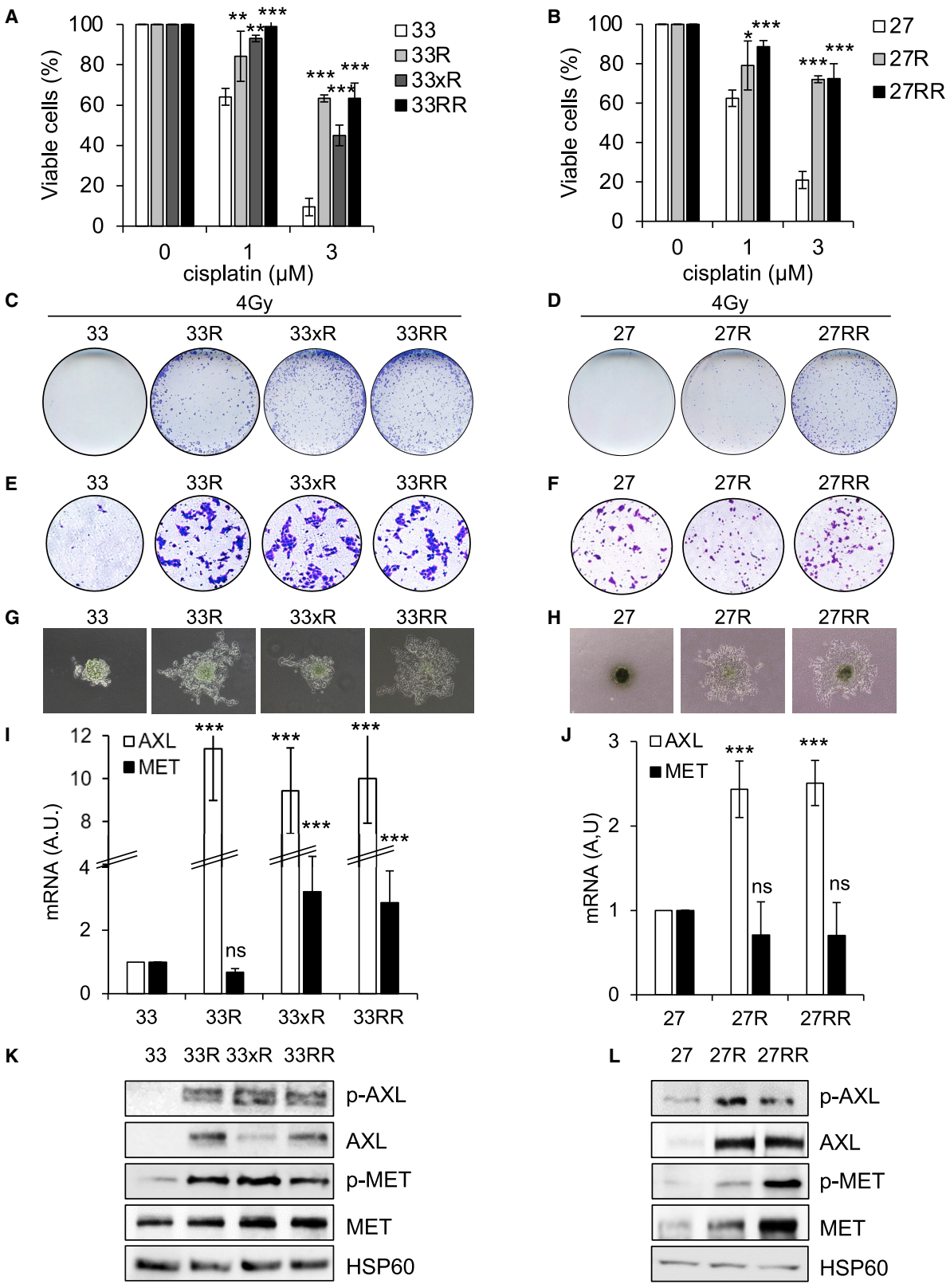

(legend on next page)

In addition, anti-angiogenic drugs (bevacizumab, axitinib, sunitinib, or sorafenib) in combination with radiotherapy have additive therapeutic effects in HNSCC.[3,9] Combining bevacizumab with chemotherapy did not improve overall survival (OS) but did improve response rate and progression-free survival (PFS) in HNSCC.

c-MET (MET) is a tyrosine kinase receptor (RTK) stimulated by hepatocyte growth factor (HGF). Activation of this pathway promotes epithelial-mesenchymal transition (EMT), a process characterized by increased cell migration, drug resistance, invasion, proliferation, and metastasis in HNSCC and other cancers.[10] MET and AXL are overexpressed in HNSCC, and their expression correlates with high-grade tumors, distant metastasis, and shorter recurrence-free survival. Proliferation, migration, and invasion of HNSCC cells depend on AXL in these tumors.[11]

Cabozantinib is a tyrosine kinase inhibitor administered *per os*. It displays a potent inhibitory activity against VEGFR2, MET, AXL, and other RTKs such as RET, KIT, and Tie2 that are involved in cancer development and progression.[12,13] Targeting these RTKs inhibits angiogenesis, tubule formation, tumor cell migration, and induces apoptosis of endothelial and tumor cells. Cabozantinib is approved for the treatment of medullary thyroid cancer, advanced renal cell carcinomas with an intermediate or poor risk and after prior VEGF-targeted therapy, and hepatocellular carcinomas previously treated with sorafenib.

Our study has shown that resistance to cisplatin and/or radiotherapy depends on overexpression of AXL and MET, leading to increased tumor aggressiveness. AXL and MET can be used as predictive markers of resistance to standard treatments and subsequent tumor recurrence. Based on these results, we proposed that cabozantinib is a relevant treatment for HNSCC patients who relapse after cisplatin and radiotherapy. We provided compelling experimental evidence for the clinical relevance of our findings.

RESULTS

HNSCC resistant cells are more aggressive and overexpress AXL and MET

Sensitive cells (CAL33 [33] and CAL27 [27]) were resistant (see STAR methods) to cisplatin (CAL33R [33R] and CAL27R [27R]; Figures 1A and 1B), radiotherapy (CAL33xR [33xR]; Figures 1C, 1D, and S1B), or both (CAL33RR [33RR] and CAL27RR [27RR]; Figures 1A–1D and S1B).

Unexpectedly, the 33R and 27R cells were also resistant to radiotherapy (Figures 1C, 1D, and S1B), and radiotherapy-resistant cells were resistant to cisplatin (Figures 1A and 1B). While we were unable to generate CAL27xR cells, we did derive 27RR cells from cisplatin-resistant cells (27R). These results suggest that resistance to cisplatin and radiotherapy is due to common molecular mechanisms.

CAL33 cells had low migratory ability, while all resistant cells (33R, 33xR, and 33RR) had high migratory ability. CAL27, 27R, and 27RR cells had the same migratory ability (Figures 1E, 1F, and S1C). 33R, 33xR, 33RR, 27R, and 27RR cells readily formed spheroids (anchorage-independent proliferation, a characteristic of aggressive tumor cells) and invaded the matrix from the spheroids. Resistant cells were more invasive compared with sensitive cells (33 and 27) (Figures 1G, 1H, and S1D).

RNA sequencing (RNA-seq) analysis showed that *AXL* was overexpressed in 33RR and 27RR cells and *MET* in 33RR cells (Figure S1A). The transcriptomic results were further verified by analyzing the levels of *AXL* and *MET* mRNA and protein. MET mRNA was upregulated only in 33xR and in 33RR cells (Figures 1I and 1J). However, MET and its phosphorylated form (p-MET) were increased in all resistant cells (33R, 33xR, 33RR, 27R, and 27RR) indicating transcriptional and post-transcriptional regulation, which ultimately led to overexpression and overactivation of MET in resistant cells (Figures 1K and 1L).

AXL mRNA and protein levels and activity (p-AXL) were increased in all resistant cells: 33R, 33xR, 33RR, 27R, and 27RR (Figures 1I–1L).

Cisplatin- and/or radiotherapy-resistant HNSCC cells therefore exhibit increased aggressiveness compared with sensitive cells, in part due to the two main drivers of cell proliferation and invasiveness, MET and AXL.

MET and AXL are overexpressed in tumors from patients at relapse on cisplatin and radiotherapy and correlate with shorter survival

Analysis of the TCGA cohort showed that mRNA levels of MET and AXL were higher in HNSCC samples compared with healthy tissue ($p < 0.0001$; Figure 2A).

In a French cohort from the Centre Antoine Lacassagne, the Nice Cancer Centre, France (n = 20; Table S1), mRNA levels of MET ($p = 0.04$) and AXL ($p = 0.015$) increased after relapse with cisplatin and radiotherapy (Figure 2B). Furthermore, in the untreated primary tumor, high levels of *MET* (median OS: 78.1

Figure 1. HNSCC resistant cells are more aggressive and overexpress AXL and c-MET

(A) Naive (33), cisplatin-resistant CAL33 (33R), irradiation-resistant CAL33 (33xR), and double-resistant (33RR) CAL33 cells were incubated with cisplatin for 48 h. Cell viability was evaluated with XTT assays. N = 4.

(B) Naive (27), cisplatin-resistant CAL27 (27R), and double-cisplatin- and irradiation-resistant (27RR) CAL27 cells were incubated with cisplatin for 48 h. Cell viability was evaluated by XTT assays. N = 4.

(C and D) 33, 33R, 33xR, 33RR, 27, 27R, and 27RR cells were irradiated with 4 Gy, and the clonogenic potential was evaluated after 10 days (see Figure S1B). N = 3.

(E and F) Serum-stimulated cell migration after 24 h was analyzed using Boyden chamber assays for 33, 33R, 33xR, 33RR, 27, 27R, and 27RR cells (see Figure S1C). N = 3.

(G and H) 33, 33R, 33xR, 33RR, 27, 27R, and 27RR cell invasion after 3 days was evaluated using spheroid assays (see Figure S1D). N = 3.

(I and J) AXL and MET mRNA levels in 33, 33R, 33xR, 33RR, 27, 27R, and 27RR cells were determined by qPCR. Control conditions were considered as the reference value (1). N = 3.

(K and L) Phospho-AXL (p-AXL), AXL, p-MET, and MET were evaluated by immunoblotting of 33, 33R, 33xR, 33RR, 27, 27R, and 27RR cells. HSP60 served as a loading control. N = 3. Statistics were performed using the ANOVA test: *$p < 0.05$, **$p < 0.01$, ***$p < 0.001$.

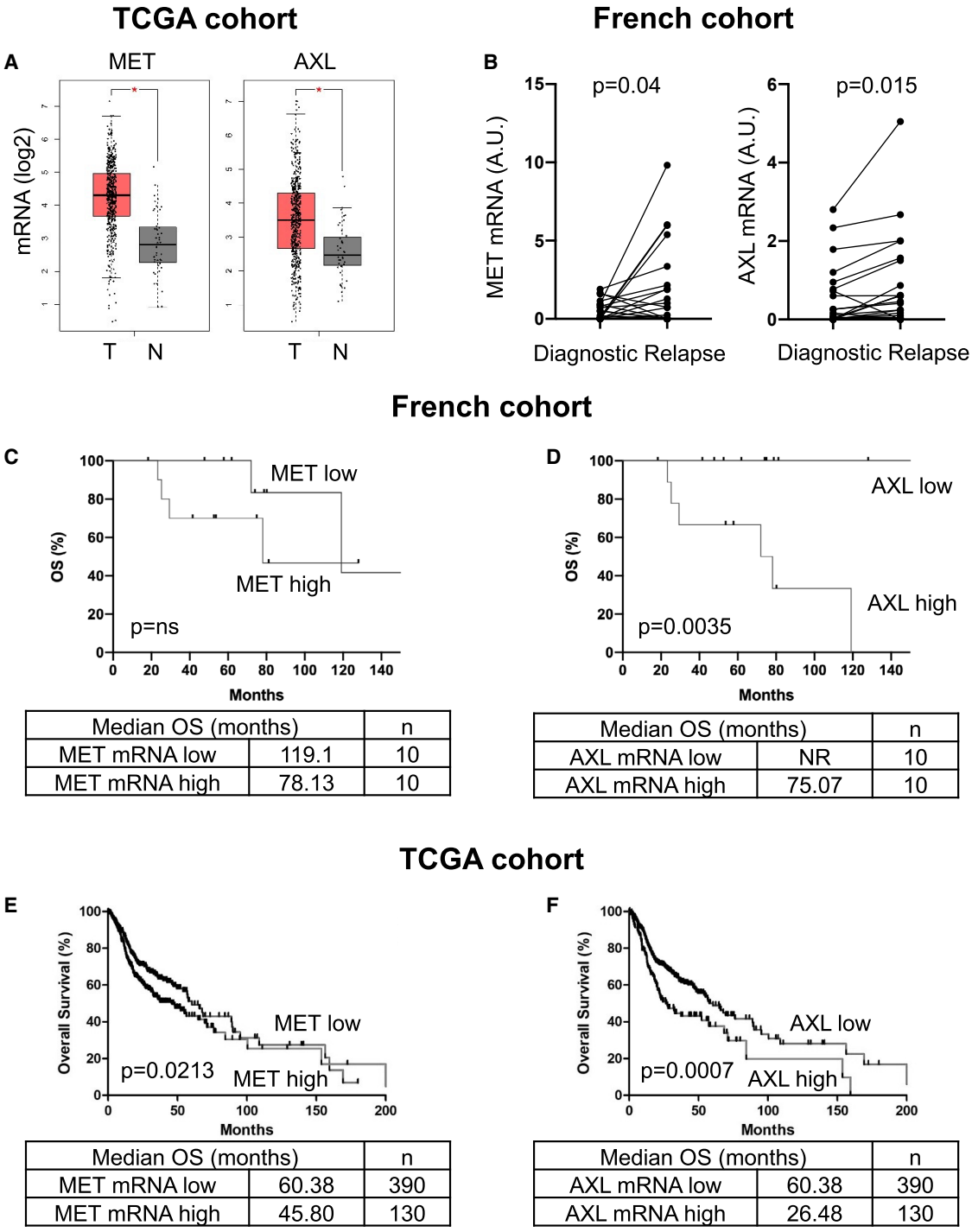

Median OS (months)		n
MET mRNA low	119.1	10
MET mRNA high	78.13	10

Median OS (months)		n
AXL mRNA low	NR	10
AXL mRNA high	75.07	10

Median OS (months)		n
MET mRNA low	60.38	390
MET mRNA high	45.80	130

Median OS (months)		n
AXL mRNA low	60.38	390
AXL mRNA high	26.48	130

Figure 2. MET and AXL are overexpressed in patient tumors following relapse after cisplatin plus irradiation and correlate with poor prognosis

(A) The levels of MET and AXL mRNAs in healthy tissue and in HNSCC (TCGA cohort) were compared.

(B) The levels of MET and AXL mRNA (qRT-PCR) in HNSCC at diagnosis were compared with the levels in HNSCC after relapse on cisplatin plus irradiation (paired samples for each patient at diagnosis and relapse, French cohort, see Table S1).

(C–F) The levels of MET (C and E) and AXL (D and F) mRNA in HNSCC patients (diagnosis) from the French (C and D) and the TCGA cohorts (E and F) correlated with OS. The Kaplan-Meier method was used to produce survival curves and analyses of censored data were performed using Cox models. Statistical significance (p values) is indicated.

versus 119.1 months, p = trend; Figure 2C) and *AXL* mRNA (median OS: 75.1 versus more than 140 months, p = 0.0035; Figure 2D) correlated with a shorter OS.

High levels of *MET* mRNA correlated with shorter disease-free survival (DFS; median: 25 versus 45 months, p = 0.15; Figure S2A) and shorter OS (median: 45.8 versus 60.4 months, p = 0.0213; Figure 2E) in samples from the TCGA cohort (n = 520). High *AXL* mRNA levels correlated with shorter DFS (median: 25.5 versus 42.8 months, p = 0.0098; Figure S2B) and shorter OS (median: 26.5 versus 60.4 months, p = 0.0007; Figure 2F). High AXL protein levels (available for 212 patients) correlated with shorter DFS (median: 18.2 versus 49.9 months, p = 0.0275; Figure S2C) and shorter OS (median: 22.8 versus 56.4 months, p = 0.048; Figure S2D).

Since the two targets of the clinically approved drug cabozantinib, AXL and MET, are overexpressed in resistant cells, we investigated the effects of other cabozantinib targets (VEGFR2 and VEGFR3) and their respective ligands (VEGF and VEGFC) on the prognosis of HNSCC. VEGF, VEGFR2, and VEGFR3 mRNA expression had no effect on DFS (Figures 2E–2G). However, high VEGFC mRNA levels correlated with shorter DFS (median: 12.2 versus 42.8 months, p = 0.027; Figure S2H).

These observations suggest that VEGFC, MET, and especially AXL are relevant markers of poor prognosis in patients with HNSCC and may represent relevant therapeutic targets for these cancers.

Cabozantinib inhibits migration and invasion of HNSCC cells

Considering the importance of MET and AXL as markers of HNSCC aggressiveness, we tested the efficacy of cabozantinib in naive and resistant HNSCC cells.

Cabozantinib inhibited the activity of AXL and MET, (p-AXL, p-MET) and two downstream signaling pathways, AKT and SRC (p-AKT and p-SRC), in 33RR and 27RR cells, respectively (Figures 3A and S3A).

Cabozantinib inhibited the migration of 33R, 33xR, and 33RR cells (Figure 3B) and cell sprouting from spheroids, a phenomenon that mimics invasion, in all resistant cells (33R, 33xR, 33RR, 27R, and 27RR; Figures 3C and S3B).

Thus, cabozantinib inhibited the aggressiveness of HNSCC cells that were sensitive or resistant to cisplatin and/or radiotherapy.

Cabozantinib decreases the proliferation and induces the death by mitotic catastrophe of HNSCC cells

Cabozantinib inhibited the clonogenic potential and reduced the viability of naive and resistant HNSCC cells (Figures 4A, 4B, and S3C–S3E).

The reduced number of viable cells prompted us to investigate the cell cycle and the effects of cabozantinib on cell death. Cabozantinib arrested the cell cycle of sensitive and resistant cells in the G2M phase (Figures 4C and S4A). This G2M arrest was accompanied by an increased number of cell nuclei (polyploidy; Figures 4D, S4B, and S4C), a phenomenon known as mitotic catastrophe.[14]

Cabozantinib decreased the expression of Plk1, one of the key events involved in mitotic catastrophe[15] (Figure 4E). The polyploid cells underwent apoptosis, which was visualized by PARP cleavage (Figures 4E and S4D) and AnnexinV/propidium iodide labeling (Figures 4F and S4E). Thus, the anti-tumor effect of cabozantinib depends on accelerated cell death by mitotic catastrophe.

These results suggest that cabozantinib is relevant as first-line therapy but also after relapse to reference treatments.

Cabozantinib has a strong anti-tumor effect on experimental HNSCC in mice

Compared with cisplatin, cabozantinib more efficiently inhibited the growth of experimental HNSCC generated from sensitive cells (CAL33; Figure 5A). It completely inhibited the growth of experimental tumors generated form resistant cells (CAL33RR; Figure 5B), while cisplatin had no effect. Tumors generated with sensitive and resistant cells and derived from mice treated with placebo (CT) or cisplatin (cis) grew significantly more than tumors from mice treated with cabozantinib (cabo) (Figure 5C). "Cabo tumors" had a high degree of necrosis (Figures 5D and S5A), lower activation of AXL and MET (p-AXL and p-MET; Figure 5E), fewer proliferating cells (Ki67 labeling; Figure 5F), and a lower number of blood vessels reaching the cells (Figure S5B). Down-regulation of *CD31* mRNA levels (Figure S5C) and a decrease in blood vessel density (CD31 staining; Figure 5G) confirmed cabozantinib-dependent inhibition of angiogenesis.

These results suggest that the dual action of cabozantinib on tumor cells and blood vessels is responsible for its anti-tumor efficacy.

Cabozantinib inhibits metastatic spread and decreases the size of existing metastases in zebrafish

Zebrafish were used as a relevant model for metastasis by studying the spread of tumor cells from the injection site to the tail.[16] In this model, 33- and 33RR cells were highly invasive, forming local metastases (Figures S6A and S6B) and metastasizing to the tail (distant metastases). After 24 h, the 33RR cells formed more distant metastases compared with the 33 cells (Figure S6C), and after 3 days, the volume of total metastases was higher (Figures S6D–S6F), indicating seeding and growth of distant metastases.

We investigated the efficacy of cabozantinib on the most aggressive cells, i.e., 33RR cells. Cabozantinib inhibited the appearance of local and distant metastases (Figures 6A and 6D). After 24 h, cabozantinib inhibited the occurence of more than 60% of distant metastases (Figure 6B) and local invasion (Figure 6C) compared with the control group.

Cabozantinib reduced the size and number of pre-existing distant metastases (Figure 6E). While the metastases from untreated zebrafish grew after 48 h, cabozantinib reduced their size by more than 50% (Figure 6F). These results strongly suggest that cabozantinib prevents metastatic dissemination and inhibits the growth of metastases.

Cabozantinib induces tumor cell death of viable tumor sections from patients with HNSCC

Surgically resected HNSCC tumors were analyzed and harvested by a pathologist (J.B.). Two biopsies from primary HNSCC and three from local recurrences after cisplatin and radiotherapy (Table S2) were used. Sections of these tumor samples (Figure 7A), in which all cells of the tumor microenvironment and tumor architecture were preserved, are a highly relevant

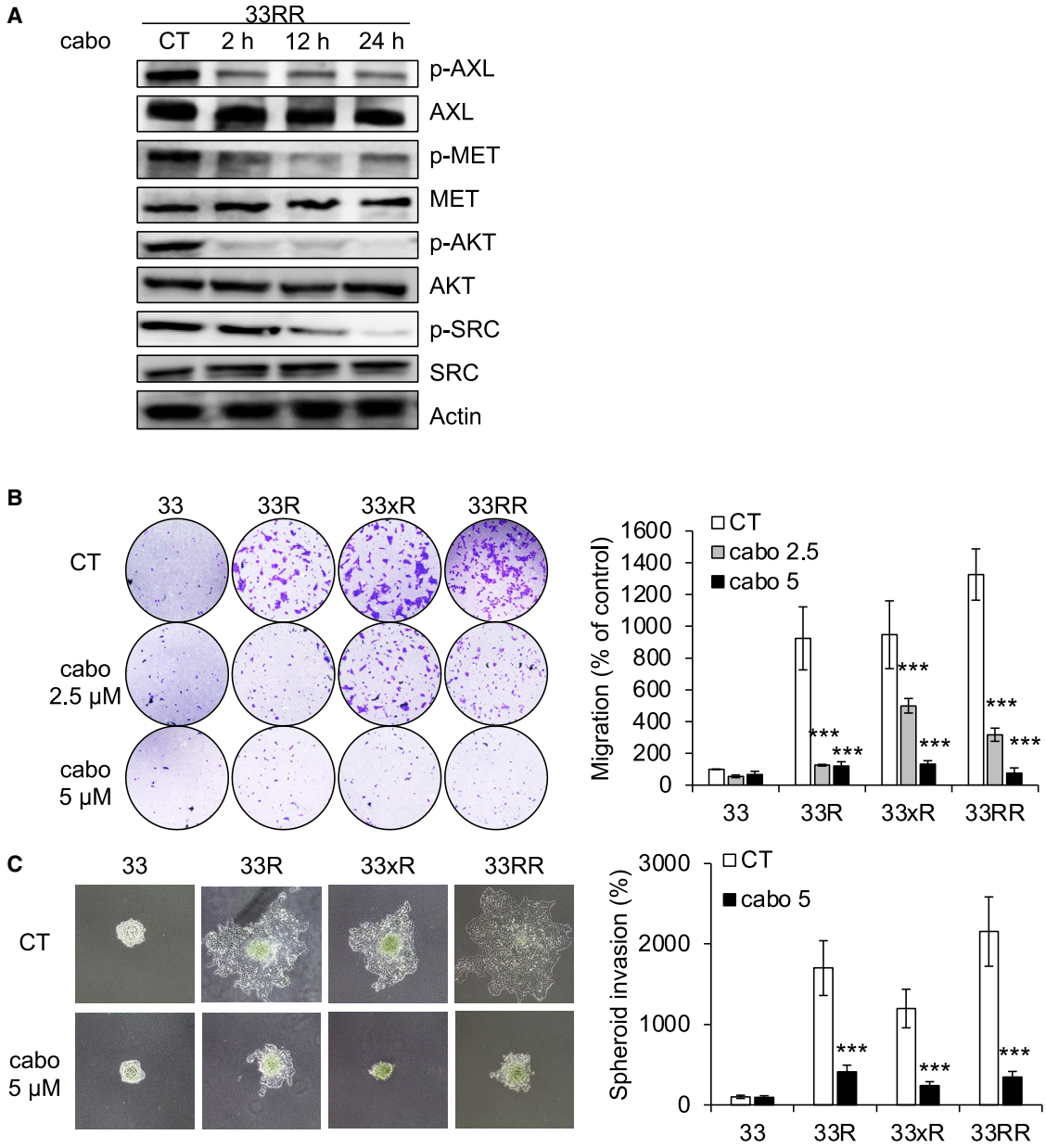

Figure 3. Cabozantinib inhibits migration, invasion, and proliferation of HNSCC cells

(A) CAL33RR cells were treated with cabozantinib (5 μM) for 1 to 24 h. p-AXL, AXL, p-MET, MET, p-AKT, AKT, p-SRC, and SCR were evaluated by immunoblotting. Actin served as a loading control. N = 3.

(B) Serum-stimulated cell migration with cabozantinib (cabo) after 24 h was analyzed using Boyden chamber assays in 33, 33R, 33xR, and 33RR cells. Representative images are shown. N = 3.

(C) 33, 33R, 33xR, and 33RR cells were treated with cabozantinib (5 μM), and cell invasion was evaluated after 3 days using spheroid assays. Representative images are shown. N = 3. Statistics were performed using the ANOVA test: *p < 0.05, **p < 0.01, ***p < 0.001.

model for evaluating the efficacy of standard or innovative therapies. These sections were treated with cabozantinib or cisplatin for 4 days, and ATP levels, which indirectly reflect cell viability, were evaluated. Cabozantinib (5 μM) decreased the tumor slice's viability more efficiently than a high concentration of cisplatin (10 μM; Figure 7B). Cabozantinib induced necrosis (H&E saffron [HES] staining; Figure 7C) and inhibited tumor cell proliferation (Ki67 staining; Figure 7D) and tumor cell death (TUNEL staining; Figure 7E) in tumor sections.

Thus, the higher anti-tumor efficacy of cabozantinib (compared with cisplatin) observed in experimental tumors (mouse and zebrafish) was confirmed in surgical specimens of human HNSCC. These results strongly suggest that cabozantinib is relevant for the treatment of HNSCC.

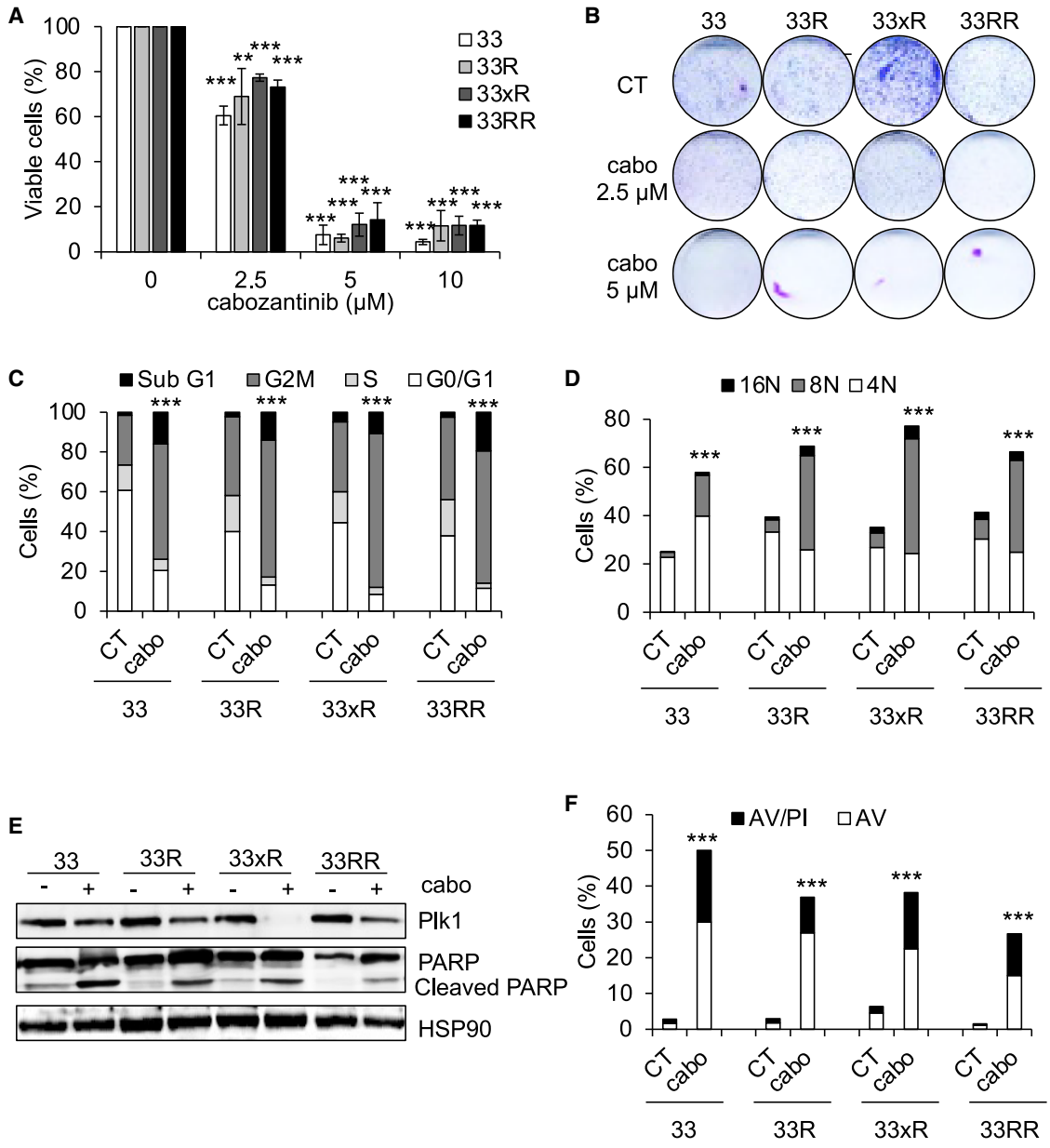

Figure 4. Cabozantinib induces cell-cycle arrest, polyploidy, and cell death

(A) 33, 33R, 33xR, and 33RR cells were treated with increasing concentrations of cabozantinib for 48 h. Viable cells were evaluated with ADAM assays. N = 4.

(B) 33, 33R, 33xR, and 33RR cells were treated with cabozantinib 2.5 or 5 μM, and clonogenic potential was evaluated after 10 days. Representative images are shown (see Figure S3D). N = 4.

(C) 33, 33R, 33xR, and 33RR cells were treated with cabozantinib 5 μM for 24 h. The cell cycle was analyzed by cytometry. N = 3.

(D–F) 33, 33R, 33xR, and 33RR cells were treated with cabozantinib 5 μM for 48 h.

(D) Cells were labeled for 15 min with propidium iodide (PI) and analyzed by flow cytometry. Histograms represent the percentage of cells with a DNA content of 4, 8, and 16N. N = 3.

(E) Plk1, PARP, and cleaved PARP (reflecting apoptosis) were detected by immunoblotting. HSP90 served as a loading control. N = 3.

(F) Cells were stained with PI/AnnexinV (AV). Histograms show AV^+/PI^- cells (apoptosis) and AV^+/PI^+ cells (post-apoptosis and/or another cell death). N = 3.

Statistics were performed using ANOVA test: $^{**}p < 0.01$, $^{***}p < 0.001$.

Cabozantinib is efficient in a multi-resistant HNSCC patient

Mr. A, a 56-year-old patient, was diagnosed with localized oropharyngeal HNSCC in 2012 and underwent oropharyngectomy. In 2015, a first locally advanced recurrence was treated with subglosso laryngectomy followed by radiotherapy. In 2019, a second recurrence was treated in irradiated fields by surgery and followed by treatment with an anti-PD1 checkpoint

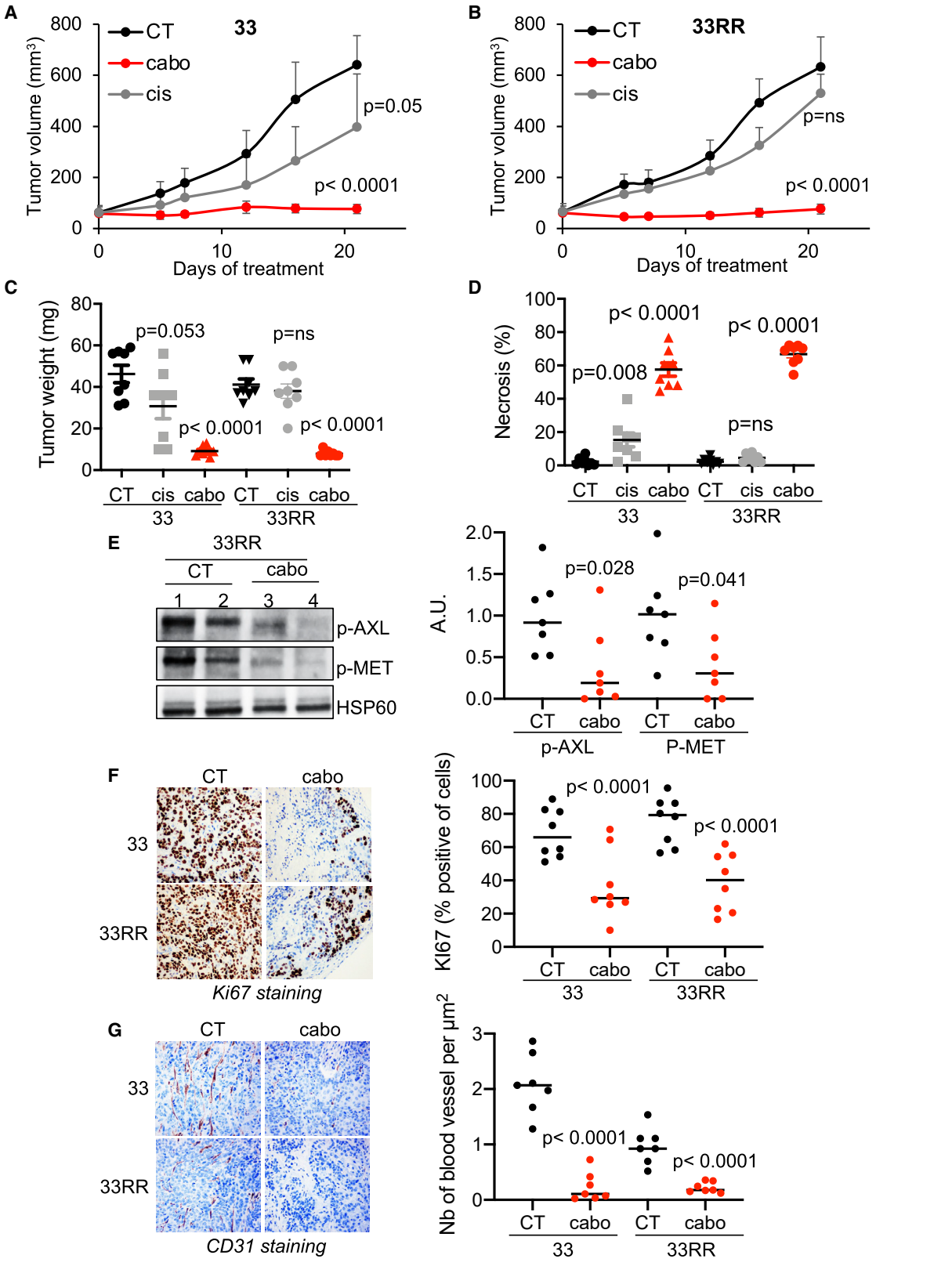

(legend on next page)

inhibitor. In October 2019, a third locally advanced recurrence was treated with palliative intent with a combination of 75 mg/m^2 cisplatin, 75 mg/m^2 docetaxel, and 400 mg/m^2 cetuximab then weekly 250 mg/m^2 for 4 cycles followed by maintenance therapy with cetuximab. In April 2020, disease progression occurred, and he was treated again with an anti-PD1 checkpoint inhibitor (May to July 2020). Molecular analyses were performed on the instructions of the molecular tumor board of the PACA-East region (Nice, France) and showed amplification of the *MET* and *CCND1* genes. As a result, he received 60 mg/day cabozantinib from January to September 2021. Between December 2020 and June 2021, stabilization followed by partial response and confirmed response was observed. In June, the dose of cabozantinib was reduced to 40 mg/day and then to 20 mg/day because of adverse events (diarrhea). Treatment was stopped after disease progression was observed in September 2021. Treatment of this patient with cabozantinib in the fifth line of treatment showed clinically significant efficacy with a 39% decrease in tumor mass (47–29 mm in the longest axis; Figure 7F). Thus, the duration of efficacy of cabozantinib in a heavily pre-treated patient with relapsed HNSCC was clinically significant.

DISCUSSION

Our study showed that the acquired resistance of HNSCC to radiotherapy and cisplatin (HNSCC cell lines and patients) depends on MET and AXL. Furthermore, high expression of MET or AXL correlates with shorter survival.

Cabozantinib is a first-in-class inhibitor of VEGFR, MET, and AXL. Promising effects of cabozantinib have been observed in various cancers, particularly metastatic renal cell carcinoma. Our results pave the way for early-stage clinical trials to validate cabozantinib as a second-line therapy for patients with HNSCC after relapse to radio/chemotherapy. In addition, the comparison of cabozantinib with cisplatin in various *in vitro* and *in vivo* models, as well as with human HNSCC samples, suggests improved efficacy of targeted therapy. Inhibition of MET and AXL, leading to reduced migration and invasion, as well as tumor cell death and inhibition of angiogenesis in response to VEGFR blockade, partly explain the anti-tumor effects of cabozantinib. Therefore, inhibition of angiogenesis alone (bevacizumab) is insufficient in such tumors and does not increase the survival rate of HNSCC patients.[17]

Like cabozantinib, other multitarget anti-angiogenic agents, such as lenvatinib, an anti-VEGFR, anti-FGFR, and anti-RET agents, have shown promising results in combination with pembrolizumab (anti-PD1) in first-line HNSCC patients.[18] A phase III clinical trial (ClinicalTrials.gov: NCT04199104) combining pembrolizumab and lenvatinib in patients with HNSCC is ongoing following encouraging results in phase IB/II.[19]

Plk1 is a mitotic kinase expressed in proliferating cells during the G2 and M phases of the cell cycle. High levels of Plk1 correlate with the aggressiveness oh HNSCC.[20] Degradation of Plk1 in a cabozantinib-dependent manner correlates with mitotic catastrophe, leading to the formation of multinucleated giant cells that eventually die by apoptosis and/or other forms of cell death.[14] Foretinib, a first-generation AXL and c-MET inhibitor, decreased the activation of PLK1 (p-PLK1), which is degraded by the proteasome. Inhibition of Plk1 led to mitotic catastrophe and therefore apoptosis of chronic myeloid leukemia cells.

Two somatic mutations of MET have been identified in HNSCC: Y1230C, known as a MET germline mutation predisposing to hereditary renal cell carcinoma, and Y1235D, leading to constitutive kinase activity.[21] Despite the low frequency of mutations in MET, overexpression of HGF and its receptor was observed in more than 80% of HNSCC. MET signaling, which is activated by HGF, leads to dimerization and phosphorylation of the receptor resulting in the recruitment of a network of intracellular adaptors and effector proteins such as phosphoinositide 3-kinase (PI3K), phospholipase Cγ 1 (PLCγ1), growth-factor-receptor-bound protein 2 (Grb2), Grb2-associated binding protein 1 (GaB1), and signal transducer and activator of transcription 3 (STAT3). Consequently, activation of MET stimulates several intracellular signaling pathways, including the PI3K/AKT, STAT3, SRC/focal adhesion kinase (FAK), and mitogen-activated protein kinase (MAPK)/ERK pathways. Activation of these pathways leads to increased cell proliferation and survival and inhibition of apoptosis, migration, invasion, and metastasis. HGF/MET signaling correlates with increased relapse rates and shorter survival of patients with HNSCC.[22,23] Furthermore, HGF/MET signaling mediates resistance to anti-EGFR inhibitors that have been added to the therapeutic armamentarium of HNSCC.

AXL, which comes from the Greek word for uncontrolled ‘‘anexelekto,’’ is an RTK that belongs to the tumor-associated macrophage (TAM) family, which also includes TYRO-3, AXL, and MER.[24] The MET-RTK family, which also includes MET and RON, has a high degree of sequence similarity to the kinase domain of AXL. The Gas6/AXL pathway mediates survival, proliferation, motility, and invasion by utilizing a diverse repertoire of signaling networks. Gas6/AXL signaling stimulates the expression of anti-apoptotic proteins such as Bcl-2 and Bcl-xL, phosphorylation, and activation of nuclear factor κB (NF-κB), the

Figure 5. Cabozantinib has a strong anti-tumor effect on experimental HNSCC in mice

5 × 10^5 CAL33 or CAL33RR cells were injected subcutaneously into the flanks of nude mice. When the tumors reached 80 mm^3, mice were treated five times a week for 4 weeks by gavage with placebo (dextrose water vehicle) or cabozantinib (40 mg/kg) or by intraperitoneal injection, three times per week with cisplatin (4 mg/kg). N = 8 mice per group.

(A and B) The tumor volume was measured twice weekly as described in the STAR methods.

(C) The tumor weight was measured at the end of the experiment.

(D) Necrosis was evaluated (HES staining).

(E) Detection of p-MET and p-AXL expression in the tumor. Representative images are shown.

(F) Ki67 immunohistochemistry (IHC) (proliferative cells). Representative images are shown.

(G) Detection of blood vessel CD31$^+$ by IHC. Representative images are shown. Statistics were performed using ANOVA test: p values are indicated.

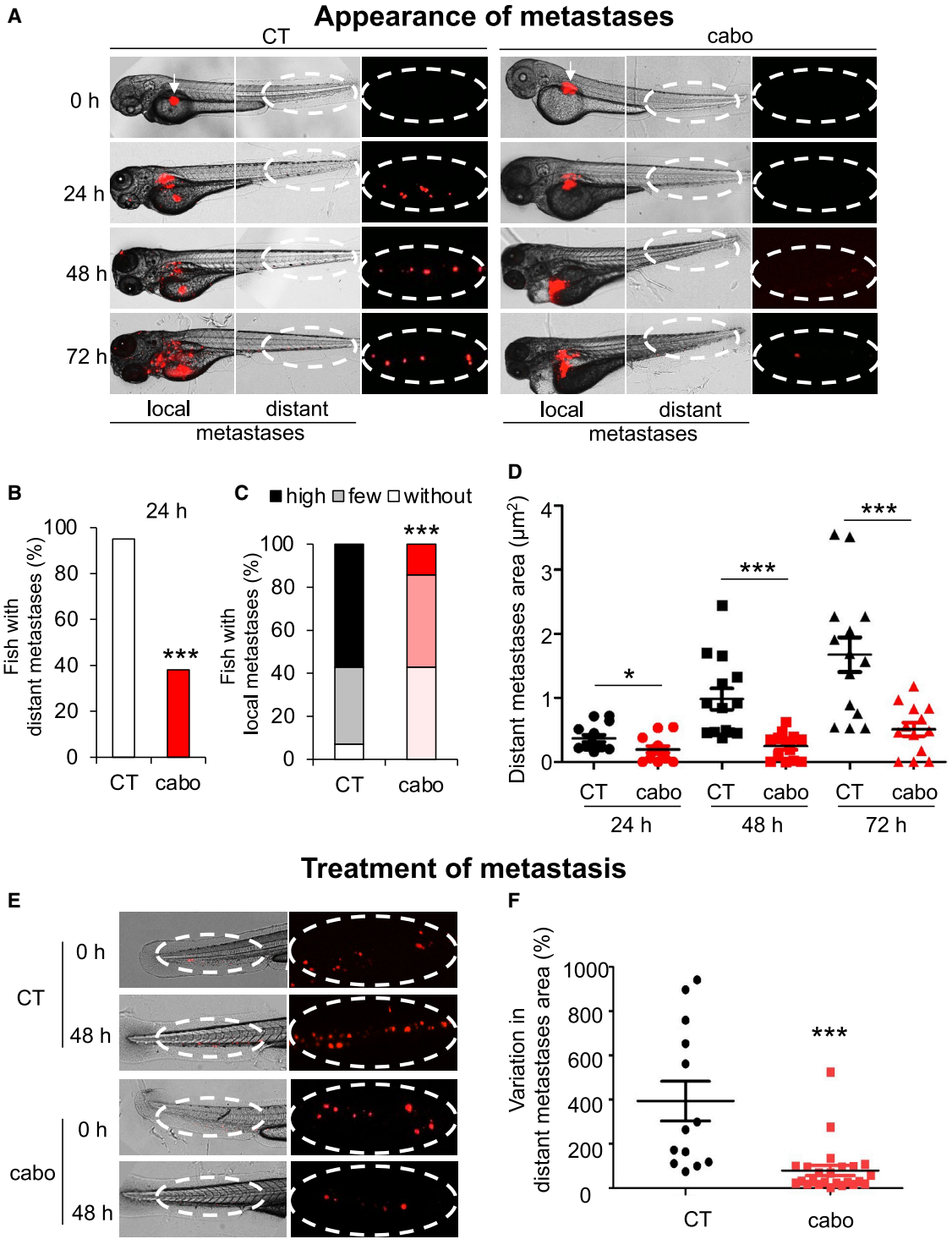

Figure 6. Cabozantinib inhibits appearance of HNSCC metastases and decreases the size of pre-existing HNSCC metastases in zebrafish

(A–D) Zebrafish embryos (N = 30) were injected with 33RR cells (labeled with red DiD) into the perivitelline space and treated with cabozantinib for 72 h (1 µM). Zebrafish embryos were monitored for tumor metastases using a fluorescent microscope. Representative images are shown, and the area of metastases was quantified.

(A) Representative images of local and distant metastases. Arrow indicates injection space at t0.

(B) Percentage of fish with distant metastases after 24 h.

(C) Evaluation of invasion of local metastases after 72 h.

(legend continued on next page)

phosphorylation and stabilization of Bad, and the inhibition of proapoptotic proteins such as caspase 3. In addition, AXL activates the MET signaling pathway.[25]

Overexpression of AXL leads to resistance to cetuximab,[26] erlotinib,[27] and radiotherapy[28] in HNSCC. Activation of AXL stimulates the PI3K pathway and induces overexpression of PD-L1, leading to resistance of HNSCC to radiotherapy.[28]

Despite the benefits of immune checkpoint inhibitors, their use as a monotherapy has been disappointing. Indeed, the efficacy of anti-PD-1 or anti-PD-L1 as monotherapy in first- and second-line treatments of recurrent or metastatic HNSCC (15%–20% objective response rate [ORR]) was modest.

Various combinations of inhibitors of angiogenesis and antibodies against PD-1 and PD-L1 antibodies are in clinical development for patients with advanced solid tumors, with promising results.

Elevated levels of local and circulating VEGF have immunosuppressive effects.[29] VEGF inhibits the differentiation of monocytes into dendritic cells and promotes the accumulation and proliferation of immunosuppressive cell types such as myeloid-derived suppressor cells (MDSCs) and regulatory T cells.

AXL excludes T cells from tumors and inhibits dendritic cell activity.[30] In experimental tumors in mice, AXL inhibits the expression of major histocompatibility complex (MHC) class I proteins and reduces the amounts of infiltrated immune cells and the cytokine production.[31] In patients with metastatic melanoma, high AXL mRNA levels correlate with resistance to anti-PD-1.[32]

HGF/MET signaling stimulates the expression of PD-L1 by tumor cells, leading to immunosuppressive effects.[33,34] *In vivo*, cabozantinib decreased the number and activity of MDSCs, impairing their ability to inhibit effector T cell proliferation, and increased infiltration of $CD8^+$ T cells into the tumor.[29]

The combination of cabozantinib and nivolumab is highly effective in the treatment of metastatic renal cell carcinoma (phase III clinical trial, interim results, median PFS = 16.6 months). Cabozantinib should reduce angiogenesis and the number of blood vessels. In addition, by inhibiting VEGFR2, AXL, and MET, cabozantinib should enhance the efficacy of anti-PD1 by increasing the number of $CD8^+$ T lymphocytes in the tumor and decreasing the number of immunosuppressive MDSCs.

Based on these hypotheses, a phase 2 clinical trial is currently underway with the combination of pembrolizumab (anti-PD-1) and cabozantinib in relapsed or metastatic HNSCC (ClinicalTrials.gov: NCT03468218). According to our results, these patients should overexpress AXL and MET (relapse after cisplatin/radiotherapy) and benefit from cabozantinib.

We also provide evidence of efficacy for cabozantinib in a multi-treated HNSCC patient. Cabozantinib was administered in the fifth line and was effective for 8 months.

In summary, our results strongly suggest that cabozantinib is very relevant for the treatment of HNSCC in relapse after radiotherapy and cisplatin. These very encouraging results require clinical validation.

Limitations of the study

Specific inhibitors of AXL (bemcentinib) and c- MET (capmatinib) or interfering RNAs targeting AXL and c-MET have been developed. They should be used to investigate the specific role of AXL and c-MET on proliferation, migration, and invasion of HNSCC cells.Cabozantinib is currently combined with pembrolizumab in clinical trials. Therefore, such a combination effect should be tested in experimental HNSCC (SCC) generated with murine HNSCC cells sensitive or resistant to cisplatin/radiotherapy in immunocompetent mice. These experiments should be relevant to evaluate the role of AXL and c-MET on cells of the tumor microenvironment.

We have shown that cabozantinib is effective in biopsy sections of patients at diagnosis and after relapse. However, the main purpose of our study was to investigate those responsible for relapse and, in particular, tumors overexpressing AXL and c-MET. Cabozantinib was tested in collaboration with the Nice Cancer Centre, France (Centre Antoine Lacassagne), in a patient who relapsed after five lines of treatment. Cabozantinib showed an impressive effect in this patient, whose PFS reached an exceptional 8 months. We believe this amazing result is much more meaningful compared with patient-derived xenograft (PDX) models.

STAR★METHODS

Detailed methods are provided in the online version of this paper and include the following:

- KEY RESOURCES TABLE
- RESOURCE AVAILABILITY
  - Lead contact
  - Materials availability
  - Data and code availability
- EXPERIMENTAL MODEL AND SUBJECT DETAILS
  - Cells
  - Zebrafish metastatic tumor model
  - Tumor xenograft experiments
  - Patients
- METHOD DETAILS
  - Cell viability (XTT)
  - Cell number - ADAM
  - Colony formation assays
  - Immunoblotting
  - Flow cytometry

(D) Quantification of the area of distant metastases during 72 h.

(E and F) Zebrafish embryos (n = 20) were injected with 33RR cells (labeled with red DiD) into the perivitelline space. Twenty-four h later, only zebrafish with metastases were chosen and treated for 48 h with cabozantinib (1 μM). Zebrafish embryos were monitored to visualize tumor spreading using a fluorescent microscope.

(E) Representative images are shown.

(F) Comparison of the area of distant metastases between the cabozantinib- and control-treated groups. Representative images are shown. Statistics were performed using the ANOVA test: *p < 0,05, ***p < 0.001.

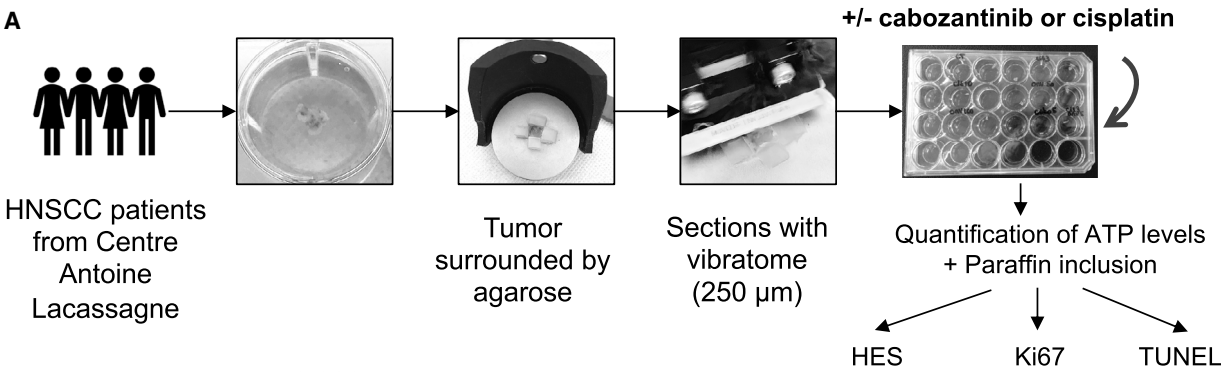

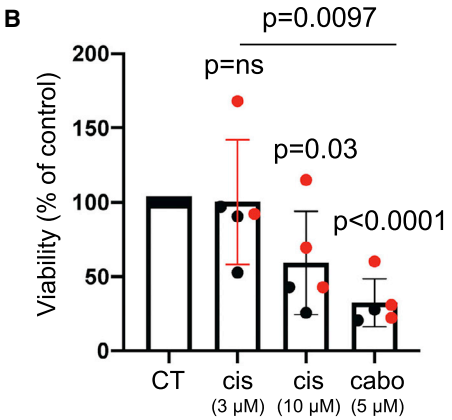

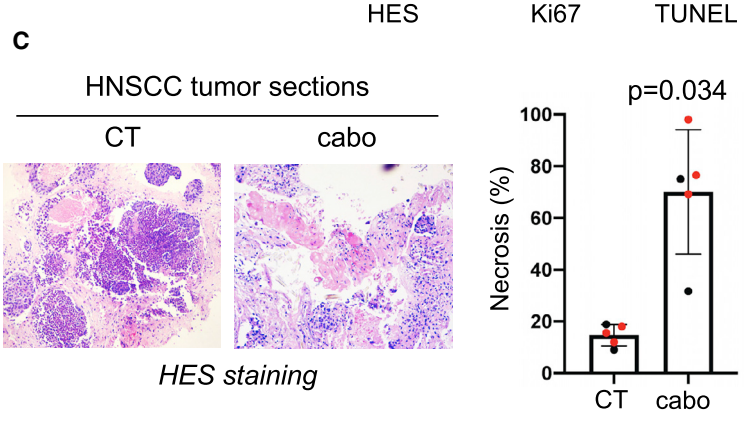

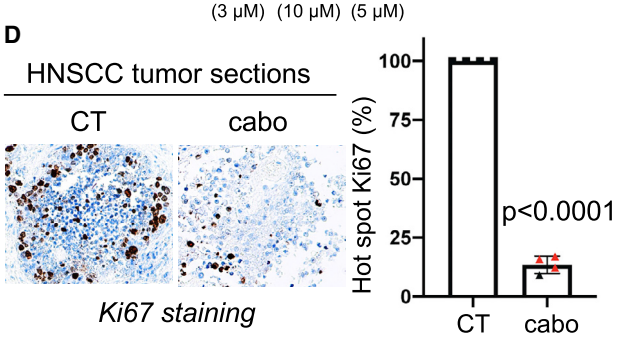

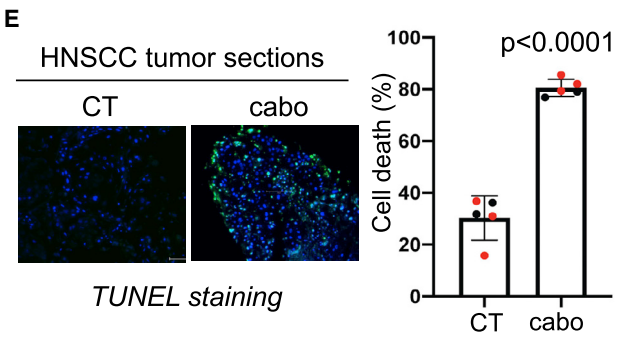

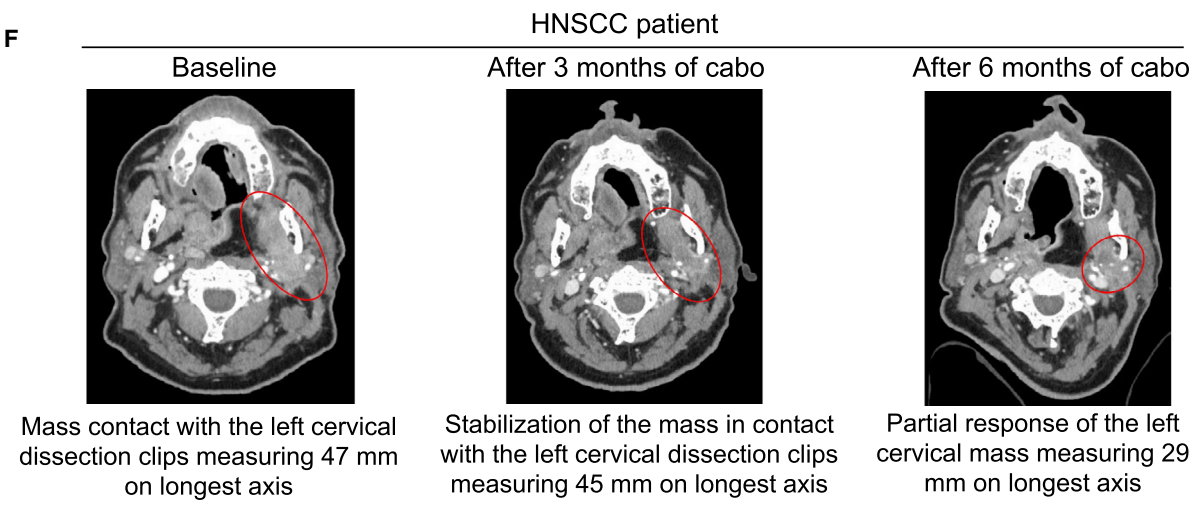

(legend on next page)

- Quantitative real-time PCR (qPCR) experiments
- Migration assays
- Tumor spheroid invasion assays
- Immunohistochemistry
- Patients

- QUANTIFICATION AND STATISTICAL ANALYSIS
  - For *in vitro* and *in vivo*
  - For patients

SUPPLEMENTAL INFORMATION

Supplemental information can be found online at https://doi.org/10.1016/j.xcrm.2022.100659.

ACKNOWLEDGMENTS

This work was supported by IPSEN funding, the French Association for Cancer Research (ARC), the Fondation de France, the Ligue Nationale contre le Cancer (Equipe Labellisée 2019), the French National Institute for Cancer Research (INCA), the National Agency for Research (ANR), and the FX Mora, Cordons de vie and Flavien Foundations. This study was conducted as part of the Centre Scientifique de Monaco Research Program, funded by the government of the Principality of Monaco. The samples and associated data were collected, selected, and made available within the "Centre de ressource biologique (CRB)" of Centre Antoine Lacassagne. We thank the IRCAN core facilities (animal and cytometry facilities) for technical help. We also thank the CHU of Nice Department of Pathology, especially Arnaud Borderie and Sandrine Destree, for technical help. To finish, we thank Ilaria Di Mauro, Valérie Kubiniek, and Valerie Duranton-Tanneur from F.P.'s laboratory.

AUTHOR CONTRIBUTIONS

Acquisition of data (provided technical assistance, provided animals, acquired and managed patient data, provided facilities, etc.), A.H., O.R., D.A., X.H., J.P., I.B., and M.D.; development of methodology, M.D.; biological resources, J.B., J.R., E.S.-B., and A.B.; conception and design, M.D. and G.P.; analysis and interpretation of data (e.g., statistical analysis), M.D.; writing – original draft, F.L., Y.C., M.D., and G.P.; review, and/or revision of the manuscript, A.H., M.D., and G.P.; supervision, project administration, and funding acquisition, M.D. and G.P.

DECLARATION OF INTERESTS

Part of this work was financed by obtaining IPSEN funding. The authors have declared that no conflict of interest exists.

Received: June 30, 2021
Revised: January 14, 2022
Accepted: May 20, 2022
Published: September 20, 2022

REFERENCES

1. Ferris, R.L., Blumenschein, G., Fayette, J., Guigay, J., Colevas, A.D., Licitra, L., Harrington, K., Kasper, S., Vokes, E.E., Even, C., et al. (2016). Nivolumab for recurrent squamous-cell carcinoma of the head and neck. N. Engl. J. Med. *375*, 1856–1867. https://doi.org/10.1056/nejmoa1602252.
2. Burtness, B., Harrington, K.J., Greil, R., Soulières, D., Tahara, M., de Castro, G., Psyrri, A., Baste, N., Neupane, P., Bratland, A., et al. (2019). Pembrolizumab alone or with chemotherapy versus cetuximab with chemotherapy for recurrent or metastatic squamous cell carcinoma of the head and neck (KEYNOTE-048): a randomised, open-label, phase 3 study. Lancet *394*, 1915–1928. https://doi.org/10.1016/S0140-6736(19)32591-7.
3. Vassilakopoulou, M., Psyrri, A., and Argiris, A. (2015). Targeting angiogenesis in head and neck cancer. Oral Oncol. *51*, 409–415. https://doi.org/10.1016/j.oraloncology.2015.01.006.
4. Jain, R.K. (2005). Normalization of tumor vasculature: an emerging concept in antiangiogenic therapy. Science *307*, 58–62. https://doi.org/10.1126/science.1104819.
5. Akervall, J., Nandalur, S., Zhang, J., Qian, C.-N., Goldstein, N., Gyllerup, P., Gardinger, Y., Alm, J., Lorenc, K., Nilsson, K., et al. (2014). A novel panel of biomarkers predicts radioresistance in patients with squamous cell carcinoma of the head and neck. Eur. J. Cancer *50*, 570–581. https://doi.org/10.1016/j.ejca.2013.11.007.
6. Gorski, D.H., Beckett, M.A., Jaskowiak, N.T., Calvin, D.P., Mauceri, H.J., Salloum, R.M., Seetharam, S., Koons, A., Hari, D.M., Kufe, D.W., and Weichselbaum, R.R. (1999). Blockage of the vascular endothelial growth factor stress response increases the antitumor effects of ionizing radiation. Cancer Res. *59*, 3374–3378.
7. Karatzanis, A.D., Koudounarakis, E., Papadakis, I., and Velegrakis, G. (2012). Molecular pathways of lymphangiogenesis and lymph node metastasis in head and neck cancer. Eur. Arch. Otorhinolaryngol. *269*, 731–737. https://doi.org/10.1007/s00405-011-1809-2.
8. Lupu-Plesu, M., Claren, A., Martial, S., N'Diaye, P.-D., Lebrigand, K., Pons, N., Ambrosetti, D., Peyrottes, I., Feuillade, J., Herault, J., et al. (2017). Effects of proton versus photon irradiation on (lymph)angiogenic, inflammatory, proliferative and anti-tumor immune responses in head and neck squamous cell carcinoma. Oncogenesis *6*, e354. https://doi.org/10.1038/oncsis.2017.56.
9. Swiecicki, P.L., Zhao, L., Belile, E., Sacco, A.G., Chepeha, D.B., Dobrosotskaya, I., Spector, M., Shuman, A., Malloy, K., Moyer, J., et al. (2015). A phase II study evaluating axitinib in patients with unresectable, recurrent or metastatic head and neck cancer. Invest. New Drugs *33*, 1248–1256. https://doi.org/10.1007/s10637-015-0293-8.
10. Moosavi, F., Giovannetti, E., Saso, L., and Firuzi, O. (2019). HGF/MET pathway aberrations as diagnostic, prognostic, and predictive biomarkers in human cancers. Crit. Rev. Clin. Lab Sci. *56*, 533–566. https://doi.org/10.1080/10408363.2019.1653821.
11. Brand, T.M., Iida, M., Stein, A.P., Corrigan, K.L., Braverman, C.M., Coan, J.P., Pearson, H.E., Bahrar, H., Fowler, T.L., Bednarz, B.P., et al. (2015). AXL is a logical molecular target in head and neck squamous cell

Figure 7. Cabozantinib is efficient on three-dimensional (3D) viable sections of surgically resected HNSCC

Samples of HNSCC obtained from patients (N = 5) following surgery were analyzed by a pathologist (HNSCC samples, Table S2). The tumor samples were surrounded by agarose, and viable 3D tumor sections (250 μm) were obtained with a vibratome. Viable 3D tumor sections were cultured in a specific medium and treated for 96 h with cabozantinib (5 μM) or cisplatin (3 and 10 μM). The results of the sections of tumors from diagnosed patients are shown in black and from patients who relapsed after cisplatin and radiotherapy are shown in red in the different panels.

(A) The experimental protocol is shown.

(B) The concentration of ATP provides a readout of the tumor section viability.

(C–E) Viable 3D tumor sections were paraffin embedded and stained with HES to quantify the areas of necrosis (C), with Ki67 to quantify cell proliferation (D), and with TUNEL to quantify apoptotic cells (E). Representative images are shown. Statistics were performed using the ANOVA test, and p values are indicated.

(F) An HNSCC patient treated with cabozantinib. Mr. A had an HNSCC and was treated in fifth line with 60 mg/day cabozantinib from January to September 2021 at the Centre Antoine Lacassagne. The tumor burden was stable form December 2020 to March 2021 followed by a partial response from March to September 2021. Computed tomography (CT) scans of the tumor mass enhanced with contrasting product are shown (baseline, after 3 months of cabozantinib, and after 6 months of cabozantinib).

carcinoma. Clin. Cancer Res. *21*, 2601–2612. https://doi.org/10.1158/1078-0432.CCR-14-2648.

12. Rathi, N., Maughan, B.L., Agarwal, N., and Swami, U. (2020). Mini-Review: cabozantinib in the treatment of advanced renal cell carcinoma and hepatocellular carcinoma. Cancer Manag. Res. *12*, 3741–3749. https://doi.org/10.2147/cmar.s202973.
13. D'Angelo, A., Bagby, S., Di Pierro, G., Chirra, M., Nobili, S., Mini, E., Villari, D., and Roviello, G. (2020). An overview of the clinical use of cabozantinib in the treatment of advanced non-clear-cell renal cell carcinoma (NCCRCC). Crit. Rev. Oncol. Hematol. *149*, 102921. https://doi.org/10.1016/j.critrevonc.2020.102921.
14. Cheng, C.-Y., Liu, C.-J., Huang, Y.-C., Wu, S.-H., Fang, H.-W., and Chen, Y.-J. (2018). BI2536 induces mitotic catastrophe and radiosensitization in human oral cancer cells. Oncotarget *9*, 21231–21243. https://doi.org/10.18632/oncotarget.25035.
15. Choueiri, T.K., Escudier, B., Powles, T., Tannir, N.M., Mainwaring, P.N., Rini, B.I., Hammers, H.J., Donskov, F., Roth, B.J., Peltola, K., et al. (2016). Cabozantinib versus everolimus in advanced renal cell carcinoma (METEOR): final results from a randomised, open-label, phase 3 trial. Lancet Oncol. *17*, 917–927. https://doi.org/10.1016/s1470-2045(16)30107-3.
16. Di Renzo, M.F., Olivero, M., Martone, T., Maffe, A., Maggiora, P., De Stefani, A., Valente, G., Giordano, S., Cortesina, G., and Comoglio, P.M. (2000). Somatic mutations of the MET oncogene are selected during metastatic spread of human HNSC carcinomas. Oncogene *19*, 1547–1555. https://doi.org/10.1038/sj.onc.1203455.
17. Wood, G.E., Hockings, H., Hilton, D.M., and Kermorgant, S. (2021). The role of MET in chemotherapy resistance. Oncogene *40*, 1927–1941. https://doi.org/10.1038/s41388-020-01577-5.
18. Kim, J.H., Kim, B.J., and Kim, H.S. (2017). Clinicopathological impacts of high c-Met expression in head and neck squamous cell carcinoma: a meta-analysis and review. Oncotarget *8*, 113120–113128. https://doi.org/10.18632/oncotarget.21303.
19. Rothenberger, N.J., and Stabile, L.P. (2017). Hepatocyte growth factor/c-met signaling in head and neck cancer and implications for treatment. Cancers *9*, 39. https://doi.org/10.3390/cancers9040039.
20. Hartmann, S., Bhola, N.E., and Grandis, J.R. (2016). HGF/Met signaling in head and neck cancer: impact on the tumor microenvironment. Clin. Cancer Res. *22*, 4005–4013. https://doi.org/10.1158/1078-0432.ccr-16-0951.
21. Xu, Y., and Fisher, G.J. (2013). Role of met axis in head and neck cancer. Cancers *5*, 1601–1618. https://doi.org/10.3390/cancers5041601.
22. Antony, J., and Huang, R.Y.-J. (2017). AXL-driven EMT state as a targetable conduit in cancer. Cancer Res. *77*, 3725–3732. https://doi.org/10.1158/0008-5472.can-17-0392.
23. Rankin, E.B., Fuh, K.C., Castellini, L., Viswanathan, K., Finger, E.C., Diep, A.N., LaGory, E.L., Kariolis, M.S., Chan, A., Lindgren, D., et al. (2014). Direct regulation of GAS6/AXL signaling by HIF promotes renal metastasis through SRC and MET. Proc. Natl. Acad. Sci. USA *111*, 13373–13378. https://doi.org/10.1073/pnas.1404848111.
24. Aguilera, T.A., Rafat, M., Castellini, L., Shehade, H., Kariolis, M.S., Hui, A.B.-Y., Stehr, H., von Eyben, R., Jiang, D., Ellies, L.G., et al. (2016). Reprogramming the immunological microenvironment through radiation and targeting Axl. Nat. Commun. *7*, 13898. https://doi.org/10.1038/ncomms13898.
25. Guo, Z., Li, Y., Zhang, D., and Ma, J. (2017). Axl inhibition induces the antitumor immune response which can be further potentiated by PD-1 blockade in the mouse cancer models. Oncotarget *8*, 89761–89774. https://doi.org/10.18632/oncotarget.21125.
26. Hugo, W., Zaretsky, J.M., Sun, L., Song, C., Moreno, B.H., Hu-Lieskovan, S., Berent-Maoz, B., Pang, J., Chmielowski, B., Cherry, G., et al. (2016). Genomic and transcriptomic features of response to anti-PD-1 therapy in metastatic melanoma. Cell *165*, 35–44. https://doi.org/10.1016/j.cell.2016.02.065.
27. Bergerot, P., Lamb, P., Wang, E., and Pal, S.K. (2019). Cabozantinib in combination with immunotherapy for advanced renal cell carcinoma and urothelial carcinoma: rationale and clinical evidence. Mol. Cancer Ther. *18*, 2185–2193. https://doi.org/10.1158/1535-7163.mct-18-1399.
28. Owusu, B., Galemmo, R., Janetka, J., and Klampfer, L. (2017). Hepatocyte growth factor, a key tumor-promoting factor in the tumor microenvironment. Cancers *9*, 35. https://doi.org/10.3390/cancers9040035.
29. Balan, M., Mier y Teran, E., Waaga-Gasser, A.M., Gasser, M., Choueiri, T.K., Freeman, G., and Pal, S. (2015). Novel roles of c-Met in the survival of renal cancer cells through the regulation of HO-1 and PD-L1 expression. J. Biol. Chem. *290*, 8110–8120. https://doi.org/10.1074/jbc.m114.612689.
30. Wagenblast, J., Hirth, D., Thron, L., Arnoldner, C., Diensthuber, M., Stöver, T., and HAMBEK, M. (2012). Effects of the Polo-like-kinase-1-inhibitor BI2536 in squamous cell carcinoma cell lines of the head and neck. Oncol. Lett. *4*, 175–177. https://doi.org/10.3892/ol.2012.700.
31. Dufies, M., Jacquel, A., Robert, G., Cluzeau, T., Puissant, A., Fenouille, N., Legros, L., Raynaud, S., Cassuto, J.P., Luciano, F., and Auberger, P. (2011). Mechanism of action of the multikinase inhibitor Foretinib. Cell Cycle *10*, 4138–4148. https://doi.org/10.4161/cc.10.23.18323.
32. Argiris, A., Li, S., Savvides, P., Ohr, J.P., Gilbert, J., Levine, M.A., Chakravarti, A., Haigentz Jr, M., Saba, N.F., Ikpeazu, C.V., et al. (2019). Phase III randomized trial of chemotherapy with or without bevacizumab in patients with recurrent or metastatic head and neck cancer. J. Clin. Oncol. *37*, 3266–3274. https://doi.org/10.1200/jco.19.00555.
33. Chen, T.H., Chang, P.M.H., and Yang, M.H. (2021). Combination of pembrolizumab and Lenvatinib is a potential treatment option for heavily pretreated recurrent and metastatic head and neck cancer. J. Chin. Med. Assoc. *84*, 361–367. https://doi.org/10.1097/jcma.0000000000000497.
34. Taylor, M.H., Lee, C.H., Makker, V., Rasco, D., Dutcus, C.E., Wu, J., Stepan, D.E., Shumaker, R.C., and Motzer, R.J. (2020). Phase IB/II trial of lenvatinib plus pembrolizumab in patients with advanced renal cell carcinoma, endometrial cancer, and other selected advanced solid tumors. J. Clin. Oncol. *38*, 1154–1163. https://doi.org/10.1200/JCO.19.01598.
35. Cerami, E., Gao, J., Dogrusoz, U., Gross, B.E., Sumer, S.O., Aksoy, B.A., et al. (2012). The cBio cancer genomics portal: an open platform for exploring multidimensional cancer genomics data. Cancer Discov. *2*, 401–404.
36. Gao, J., Aksoy, B.A., Dogrusoz, U., Dresdner, G., Gross, B., Sumer, S.O., et al. (2013). Integrative analysis of complex cancer genomics and clinical profiles using the cBioPortal. Sci Signal. *6*. https://doi.org/10.1126/scisignal.2004088.

STAR★METHODS

KEY RESOURCES TABLE

REAGENT or RESOURCE	SOURCE	IDENTIFIER
Antibodies		
Phospho-AXL	Cell Signaling	RRID:mAb#5724
Phospho-MET	Cell Signaling	RRID:mAb#3077
Phospho-AKT	Cell Signaling	RRID:mAb#9271
Phospho-SRC	Cell Signaling	RRID:mAb#2101
AXL	Santa Cruz	RSC-166269
MET	Invitrogen	RRID:t 37-0100
AKT	Cell Signaling	RRID:mAb#9272
SRC	Cell Signaling	RRID:mAb#2109
Plk1	Abcam	RRID:ab17056
HSP90	Cell Signaling	RRID:mAb#4877
HSP60	Cell Signaling	RRID:mAb#12165
PARP	Cell Signaling	RRID:mAb#9532
anti-mouse CD31 (clone MEC 13.3)	BD Pharmingen	RRID:550274
Ki67 (clone MIB1)	DAKO	RRID:GA626
Biological samples		
HNSCC samples at diagnosis and at relapse in parrafin	Human donors	Centre Antoine Lacassagne
HNSCC fresh biopsies	Human donors	Centre Antoine Lacassagne
Chemicals, peptides, and recombinant proteins		
Cabozantinib (BMS-907351)	Selleckchem	Cat# S1119
Cisplatin	Mylar	Centre Antoine Lacassagne Pharmacy
Tricaine	Sigma-Aldrich	Cat# MS-222
Annexin V-APC	Biolegend	Cat#640941
Propidium Iodide	Biolegend	Cat#421301
ECL	Millipore	Cat#WBKL50500
FBS	Dutscher	Cat#S1810-500
GIEMSA	Sigma-Aldrich	Cat#GS1L-1L
Vybrant DiD cell-labeling solution	LifeTechnologies	Cat# V22887
Critical commercial assays		
XTT (Cell Proliferation kit II)	Roche	Cat# 11465007001
Pierce™ BCA Protein Assay Kit	Thermo Fisher Scientific	Cat# 23225
QuantiTect Reverse Transcription Kit	Qiagen	Cat# 205311
SYBR Master Mix Plus	Eurogentec	Cat# UF-RSMT-B0701
In Situ Cell Death Detection Kit	Roche	Cat# 11684795910
ATP Bioluminescence Assay Kit HSII	Roche	Cat# 11699695001
Matrigel® Matrix	Corning	Cat# 356237
Collagen I	Corning	Cat# 354249
Deposited data		
HNSCC patients - mRNA analysis	TCGA	www.cbioportal.org, TCGA HNSCC Firehose Legacy cohort[38,39]
Experimental models: Cell lines		
CAL33	Centre Antoine Lacassagne, DSMZ	Cat# ACC 447
CAL27	Centre Antoine Lacassagne, ATCC	Cat# CRL-2095

(*Continued on next page*)

Continued

REAGENT or RESOURCE	SOURCE	IDENTIFIER
Experimental models: Organisms/strains		
Zebrafish embryos	Karolinska institute, Sweden	N/A
Rj:NMRI-Foxn1nu/Foxn1nu female mice	Janvier Labs, France	N/A
Oligonucleotides		
AXL	Sigma-Aldrich	R-ATCTCTTGGTACTCAGATACTC
		F-CATGAAACATGGAGACCTAC
MET	Sigma-Aldrich	R-ATCTCTTCCCAGTGATAACC
		F- CATGTGAATTTTCTCCTGGAC
Software and algorithms		
Prism 8.0	GraphPad	https://www.graphpad.com
ImageJ	Fiji	https://imagej.nih.gov/ij/
Other		
DMEM high glucose GlutaMAX™ Supplement Pyruvate	Thermo Fisher Scientific	Cat# 31966-021
Penicillin streptomycin Gibco® Life Technologies	Thermo Fisher Scientific	Cat# 15140122
Normocure™	Invivogen	Cat# ant-noc
Airway Epithelial Cell Growth Medium	Promocell	Cat# C-21060
PVDF membrane	Millipore	Cat# T831.1
cell culture inserts with 8.0 μm pore transparent PET membrane	Corning, Falcon	Cat# 353097

RESOURCE AVAILABILITY

Lead contact

Further information and requests for resources and reagents should be directed to and will be fulfilled by the lead contact, Maeva Dufies (maeva.dufies@gmail.com).

Materials availability

All unique/stable reagents generated in this study are available from the lead contact with a completed materials transfer agreement.

Data and code availability

The published article includes all datasets generated or analyzed during this study. This paper does not report original code. Any additional information required to reanalyze the data reported in this work paper is available from the lead contact upon request, Maeva Dufies (maeva.dufies@gmail.com).

EXPERIMENTAL MODEL AND SUBJECT DETAILS

Cells

CAL27 HNSCC cells were purchased from the American Tissue Culture Collection. CAL33 HNSCC cells were purchased from DSMZ. CAL27R and CAL33R are cisplatin resistant cells and were obtained by chronic exposure to increasing concentrations of cisplatin up to 10 μM CAL33xR cells are resistant to irradiation and were obtained with 25 rounds of 8 Gy irradiation. CAL33RR and CAL27RR cells are resistant to cisplatin and irradiation and were obtained from CAL33R and CAL27R cells and after 25 rounds of 8 Gy irradiation.

Cells were cultured in DMEM high glucose, GlutaMAXTM Supplement, pyruvate – (Thermo Fisher Scientific) and supplemented with 7% FCS and 0.1% penicillin streptomycin (10 000 μg/mL, Gibco® Life Technologies).

Zebrafish metastatic tumor model

All animal experiments were approved by the Northern Stockholm Experimental Animal Ethical Committee. Zebrafish embryos were raised at 28°C under standard experimental conditions. Zebrafish embryos at the age of 24 hpf were incubated in aquarium water containing 0.2 mmol/L 1-phenyl-2-thio-urea (PTU, Sigma). At 48-hpf, zebrafish embryos were dechorionated with a pair of sharp-tip forceps and anesthetized with 0.04 mg/mL of tricaine (MS-222, Sigma). Anesthetized embryos were subjected to microinjection. CAL33RR tumor cells were labeled with a Vybrant DiD cell-labeling solution (LifeTechnologies). Tumor cells were resuspended in PBS and approximately 5 nL of the cell solution was injected into the perivitelline space (PVS) of each embryo by an Eppendorf micro-injector (FemtoJet 5247). Non-filamentous borosilicate glass capillarie needles were used for injection. The injected zebrafish

embryos were transferred into PTU aquarium water. For Figure 6, fish were treated with cabozantinib (1 μM). For Figure 7, 24 h after injection, only zebrafish with metastases were chosen and treated with cabozantinib (1 μM). Zebrafish embryos were monitored for 72 h to investigate tumor metastasis using a fluorescent microscope (Nikon Eclipse 90).

Tumor xenograft experiments

5×10^5 CAL33 or CAL33RR cells were injected subcutaneously into the flanks of 5-week-old nude (nu/nu) female mice (Janvier, France). The tumor volume was determined with a caliper ($v = L*l^2*0.5$). When the tumor reached 80 mm^3, mice were treated five times a week for 4 weeks, by gavage with placebo (dextrose water vehicle), cabozantinib (40 mg/kg) or by intraperitoneal injection three times per week with cisplatin (4 mg/kg). This study was carried out in strict accordance with the recommendations of the Guide for the Care and Use of Laboratory Animals. Our experiments were approved by the ''Comité national institutionnel d'éthique pour l'animal de laboratoire (CIEPAL)'' (reference: 2018102510495275 – PEA 535) to ensure that the use of animals complies with all applicable legislation and following the 3R's principle. At the end of the experiment, blood from mice was drawn. The blood formula was tested using Hemavet (HV950FS - Drew Scientific) after treatments (alone or combined).

Patients

Informed consent was obtained from all individual participants included in the study. All patients gave written consent for the use of tumor samples for research. This study was conducted in accordance with the Declaration of Helsinki (Centre Antoine Lacassagne Biological Resource Center). Human subject characteristics are provided in Tables S1 and S2, and include data on gender, on TNM status and tumor location for each diagnostic group.

METHOD DETAILS

Cell viability (XTT)

5×10^3 cells were incubated in 96-well plates with different effectors for the times indicated in the figure legends. 50 μL of sodium 3′-[1-phenylaminocarbonyl)-3,4-tetrazolium]-bis(4-methoxy-6-nitro) benzene sulfonic acid hydrate (XTT) was added to each well (Roche). The assay is based on the cleavage of the yellow tetrazolium salt XTT to form an orange formazan dye by metabolically active cells. Absorbance of the formazan product, reflecting cell viability, was measured at 490 nm. Each assay was performed in quadruplicate.

Cell number - ADAM

Cell viability and cell death was assessed using the ADAM-MC apparatus (NanoEnTek, Guro-gu, Seoul, Korea) based on fluorescent propidium iodide staining according to the manufacturer's instructions. 50 μL of cell sample were mixed with an equal volume of AccuStain Solution T for total cell counting or AccuStain Solution N for non-viable cell counting. The number of viable cells was next evaluated (T-N).

Colony formation assays

HNSCC cells (3000 cells per condition) were treated or not with cabozantinib (BMS-907351, Cat No.S1119). Colonies were detected after 10 days of culture. Cells were then washed, fixed and stained with GIEMSA (Sigma). Pictures were then taken.

Immunoblotting

Cells were lysed in buffer containing 7.5% SDS, 30% glycerol, 0.3 M Tris pH6.8. 30 to 50 μg of proteins were separated on 10% SDS-PAGE, transferred onto a PVDF membrane (Immobilon, Millipore) and then exposed to the appropriate antibodies. Proteins were visualized with the ECL system using horseradish peroxidase-conjugated anti-rabbit or anti-mouse secondary antibodies. The following primary antibodies were used: Plk1 (Abcam, ab17056, mouse), phospho-AXL (Cell signaling, #5724S), phospho-MET (Cell signaling, #3077S), phospho-AKT (Cell signaling, #9271S), phospho-SRC (Cell signaling, #2101S), AKT (Cell signaling, #9272) SRC (Cell signaling, #2109S), AXL (Santa Cruz,), MET (Invitrogen, 37-0100), PARP (Cell signaling, #9532), HSP90 (Cell signaling, #4877) and HSP60 (Cell signaling, #12165).

Flow cytometry

Analysis of apoptosis

Following incubation with cabozantinib, 100 000 cells were washed with ice-cold PBS, centrifuged, and stained in PBS 400 μL with the Annexin-V-APC (Biolegend, 2 μL) and propidium iodide (PI, Biolegend, 10 μL) during 15 min. Fluorescence was measured using the FL2 and FL3 channels of a fluorescence-activated cell sorter apparatus (FACS-Calibur cytometer).

Cell cycle analysis

After treatment, cells were washed, fixed in ethanol 70% and, finally, left overnight at −20°C. Cells were next incubated in PBS 400 μL, RNase A 3 μg/mL and PI 10 μL (Biolegend) for 30 min at 4°C. Cellular distribution across the different phases of the cell cycle or DNA content was analyzed with a FACS-Calibur cytometer.

Quantitative real-time PCR (qPCR) experiments

1 μg of total RNA was used for the reverse transcription, using the QuantiTect Reverse Transcription kit (QIAGEN, Hilden, Germany), with a blend of oligo (dT) and random primers to prime first-strand synthesis. SYBR master mix plus (Eurogentec, Liege, Belgium) was used for qPCR. The mRNA level was normalized to 36B4 mRNA.

Migration assays

8×10^4 cells were seeded into the top chamber of cell culture inserts with 8.0 μm pore transparent PET membrane (Corning, Falcon, Cat No: 353097) in medium without FBS, while medium with 10% FBS was present in the bottom chamber. After 24 h, media and remaining cells were removed from the top chamber. Inserts were fixed with 3% PFA. Cells that migrated through the filter and adhered to the lower surface were stained for 10 min with 0.5% crystal violet in 25% ethanol and were analyzed and quantified.

Tumor spheroid invasion assays

A cell suspension of 1.5×10^4 cells/mL was prepared and 200 μL of this suspension were seeded in 24 wells containing solidified agarose 1% incubated at 37°C for 48 h. Spheroids containing 3000 cells each were placed on the inside face of the cover of a culture dish and incubated at 37°C. Formed spheroids were transferred into 12 wells containing 50 μL of the following mix: 200 μL matrigel (Corning® Matrigel® Matrix), 100 μL collagen I (8 mg/mL; corning), 80 μL HEPES 1 M and 320 μL DMEM 7% FCS and grown for the designated time. The diameters of spheroids were monitored with a EVOS optical microscope. Cell invasion through the surrounding matrigel/collagen was measured using ImageJ software and the final spheroid size was compared to the initial size at time zero.

Immunohistochemistry

Sections of formol-fixed and paraffin-embedded tumors were stained with HES and necrotic area were quantified. Sections were incubated with anti-mouse CD31 (clone MEC 13.3, BD Pharmingen, diluted at 1:500) or Ki67 (clone MIB1, DAKO, Ready to use) antibodies.

Patients

Informed consent was obtained from all individual participants included in the study. All patients gave written consent for the use of tumor samples for research. This study was conducted in accordance with the Declaration of Helsinki (Centre Antoine Lacassagne Biological Resource Center). Human subject characteristics are provided in Tables S1 and S2, and include data on gender, on TNM statuts and tumor location for each diagnostic group.

HNSCC patients from Centre Antoine Lacassagne - Treatment of primary HNSCC viable 3D sections

Five HNSCC tumor specimens obtained just after surgery were provided through collaboration with the Centre Antoine Lacassagne (Pr A. Bozec). Viable tumor sections (250 μm, tumor samples were confirmed by a pathologist (Dr J. Boyer)) were obtained with a vibratome HM650V machine. They were seeded in Airway Epithelial Cell Growth Medium (PromoCell) supplemented with NormocureTM (Invivogen) and treated with a range of cabozantinib or cisplatin concentrations. Tumor sections were then paraffin-embedded and analyzed using HES for the quantification of necrotic areas and TUNEL staining (*In Situ* Cell Death Detection Kit, sigma) for the quantification of dead cells. Tumor sections were lysed and the ATP concentration evaluated (ATP Bioluminescence Assay Kit HSII, Roche), normalized to the protein concentration and represented as a read-out of viability (see Figure 7 and Table S2).

French cohort: HNSCC patients from the Centre Antoine Lacassagne – mRNA analysis

The mRNA level of different genes was analyzed by qRT-PCR in tumor/metastasis, for the same patients, at diagnosis and at relapse after cisplatin and radiotherapy for twenty HNSCC patients (see Table S1). OS was calculated from patient subgroups with mRNA levels that were less or greater than the median value.

TCGA cohort: HNSCC patients - mRNA analysis

Normalized RNA sequencing (RNA-Seq) data produced by The Cancer Genome Atlas (TCGA) were downloaded from cBioportal (www.cbioportal.org, HNSCC TCGA Firehose Legacy cohort, RNA-Seq V2).[35,36] Data were available for 530 HNSCC tumor samples TCGA subjected to mRNA expression profiling. DFS and OS were calculated from patient subgroups with mRNA levels (z-score) that were less or greater than the third quartile value.

QUANTIFICATION AND STATISTICAL ANALYSIS

For *in vitro* and *in vivo*

Statistical analyses were performed with Prism 8 software. Datas are expressed with mean +/− the standard error (SEM). Significance was determined with the Student's *t*-test. The ANOVA with Bonferroni post hoc test was used for multiple comparisons.

For patients

The Student's *t*-test was used to compare continuous variables and the chi-square test, or Fisher exact test (when the conditions for use of the χ^2-test were not fulfilled), were used for categorical variables. DFS was defined as the time from surgery to the appearance of metastasis. OS was defined as the time between surgery and the date of death from any cause, censoring those alive at the last follow-up. The Kaplan-Meier method was used to produce survival curves and analyses of censored data were performed using Cox models.